Fachtagung "Experimentelle Strömungsmechanik"
6. – 8. September 2016, Cottbus

Turbulente Geschwindigkeitsfelder in einer rechteckigen Konvektionszelle mit großem Aspektverhältnis: Vergleich zwischen Experiment und Simulation

Velocity field in rectangular large-aspect-ratio turbulent convection cells: Comparison between experiment and simulation

Christian Kästner, Anastasiya Kolchinskaya, Max Körner, Dmitry Krasnov, Christian Resagk & Jörg Schumacher

Institut für Thermodynamik und Fluidmechanik, Technische Universität Ilmenau, Am Helmholtzring 1, 98693 Ilmenau

Konvektion, Turbulenz, PIV, DNS
Convection, turbulence, PIV, DNS

Abstract

We report a one-to-one comparison of an experimental and numerical analysis of the horizontal velocity field in turbulent Rayleigh-Bénard convection, applied to a rectangular convection cell with aspect ratio $\Gamma \approx 10$ and air as a working fluid. Horizontal cuts through the convective flow were obtained from 2d particle image velocimetry (PIV) measurements. Optical access for laser light sheet and PIV camera was provided by transparent sidewalls and a transparent heating plate. The PIV data contained both horizontal velocity components in planes at different heights, close to the cooling plate as well as in the mid-plane of the cell, at Rayleigh number $Ra = 5\times10^5$.

These results were compared with data obtained from direct numerical simulations (DNS) applying a finite difference method. The analysis revealed good agreement between experiment and simulation.

Introduction

Thermal convection is characterized by heat and mass transport due to thermally induced density fluctuations within a fluid. A common standardized model experiment is the Rayleigh-Bénard convection, applied by a convection cell which is heated from below and cooled from above, and closed by adiabatic side walls.[1,2,3] Due to the different temperatures of top and bottom enclosure buoyancy force leads to a directed flow of the fluid. Depending on the temperature gradient the convective flow develops from laminar, over convection with increasing complexity, to fully turbulent with increasing temperature gradient. The degree of thermal driving is characterized by the dimensionless Rayleigh number Ra, defined as $Ra = \alpha \Delta T g h^3 / \nu a$; α: thermal expansion coefficient, ΔT: temperature difference between hot and cold enclosure, g: acceleration due to gravity, h: height of the convection cell, ν kin-

Karlsruhe, Germany, ISBN 978-3-9816764-2-6

ematic viscosity and *a*: thermal diffusivity.[4] A common method to investigate the flow of mass is to seed the fluid with particles that can be tracked with optical recording systems. The knowledge of particle displacement and corresponding lapse of time enables the calculation of velocity vectors. Two possibilities are available: particle tracking velocimetry (PTV) which tracks single particles and particle image velocimetry (PIV) which tracks a cloud of particles. Both methods require optical access to the convective flow since the particles are illuminated and Mie-scattered light is observed. Several applications were developed, planar PIV/PTV where the flow is illuminated with a laser light sheet, yielding 2-dimensional field of flow, and volumetric methods like Stereo- or Tomo-PIV where the complete volume is illuminated and 3-dimensional flow information is obtained.[5,6,7,8,9]

The geometry (aspect ratio) of a convection cell is the most limiting parameter for yielding large *Ra* and reasonable optical access to the convective flow. Hence large aspect ratios lead to serious challenges for measuring particle trajectories (as well as the application of large Rayleigh numbers). Various possibilities of optical access to large aspect ratio convection cells are sketched in Figure 1 and are discussed in the following. A commonly applied method to observe the convective field is to look through a transparent window inside the cooling plate. But in this case the field of view is reduced (see Figure 1 a) which makes this method exclusively applicable for small aspect ratio cells, despite the fact that the glass window leads to thermal disturbance of the convection (non-isothermal condition of the cooling plate). Alternatively, since the heating and cooling plate of a standard convection cell are usually non-transparent, optical access can thus only be applied through a lateral window from the side which makes optical observation of the horizontal plane of flow as more complicated as the cell height is shrunk. Consequently, the observation angle between the horizontal plane of flow and the viewing normal of an observing camera converge to zero, which makes large aspect ratios technically not accessible without losing accuracy (see Figure 1 b). The only opportunity to make things right is to shift the camera's field of view opposite to the horizontal plane of flow, yielding orthogonal geometry of camera's viewing normal to flow plane as shown in Figure 1 c), by applying a transparent heating plate (or a transparent cooling plate – not discussed here). Hence the horizontal plane of view is accessible with sufficient accuracy, obviously larger than obtained in small aspect ratio convection cells under standard conditions. The "only" two requirements of the transparent heating plate are transparency within the wavelength range of observation and the homogeneity of temperature distribution, namely isothermal property, along the surface of the heating plate. This can be realized by a glass plate coated with a transparent conductive oxide (TCO).[10,11] The heating of the plate is thus simply generated due to Joule heating of electrical current flowing through the sheet resistance of the TCO. For sure there are further solutions to be presented in the near future since horizontal flow visualization in large aspect ratio convection cells is of great research interest. On these grounds, we developed a rectangular Rayleigh-Bénard cell with transparent heating plate to get full access to the 2-dimensional velocity field in horizontal planes. Therefore, planar PIV was applied to measure time-series of the velocity fields. Hence the experimental results were compared to direct numerical simulations (DNS), applying a second-order finite-difference method.[12,13]

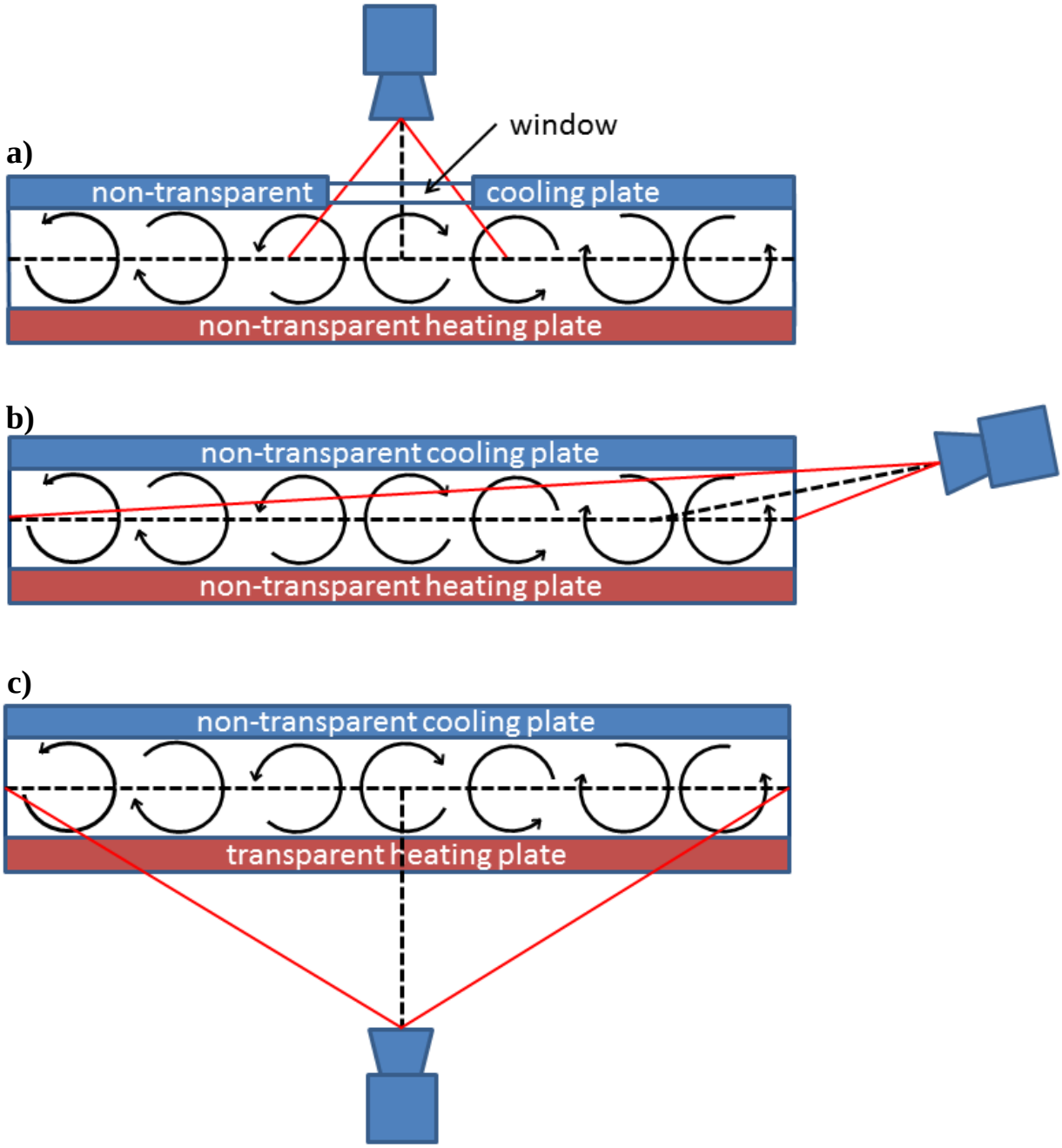

Figure 1: Rayleigh-Bénard experiment at large aspect ratio; a) standard methodology to look through a window inside the non-transparent cooling plate, and b) geometric problem of standard methodology to visualize the horizontal field of flow from the side, and c) visualization through a transparent heating plate.

Initially, we checked the applicability of a commercial transparent heating plate with respect to transparency and isothermal property to build up a suitable Rayleigh-Bénard cell, yielding new insights into large aspect ratio thermal convection and respective flow pattern.

Experimental

For studying turbulent Rayleigh-Bénard convection in air we used a closed square cell with dimension of 460 × 460 × 46 mm³ yielding an aspect ratio of $\Gamma = 10$. The transparent almost adiabatic side walls were made of 5 mm thick poly(methyl metacrylate) (PMMA). The transparent bottom heating plate HVT-2 (Hillesheim GmbH) had a maximum heating power of about 1600 W at 230 V. The heating power was controlled with an infinitely variable DC power supply (EA ELEKTRO-AUTOMATIK EA-PS 9080-100). The nontransparent cooling plate (ELKOM ÖKOTHERM-PLUS) was driven by a recirculating cooler (Julabo F32HP). Surface temperatures of the hot and cold enclosure were measured each with four PT100 resistance thermometers (UST Umweltsensortechnik GmbH) located close to the edges of the cell, 20 mm away from the walls. The PT100s were fixed with two component adhesive (JB Weld) and connected to a data logger (Agilent 34970A) due to a 20 channel multiplexer (Agilent 34901A).

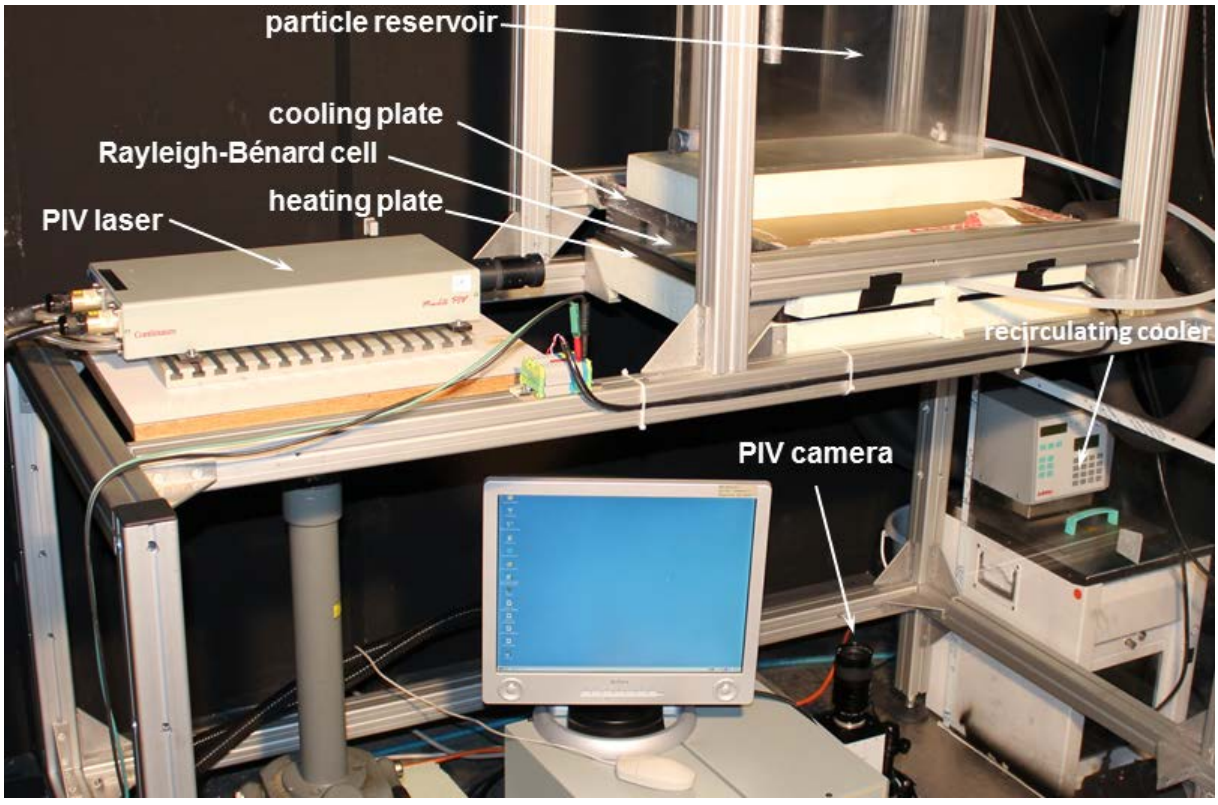

Figure 2: Experimental setup: Rayleigh-Bénard cell containing heating and cooling plate, seeding particle buffer tank, PIV light sheet laser and camera.

Velocity fields were obtained by PIV. Laser light sheet was applied due to a double pulse laser (continuum Minilite PIV) at 18 mJ pulse energy, 1 Hz repetition rate and 10 ms pulse separation time, equipped with light sheet optics (Linos). Double frames were recorded with a CCD camera (PCO SensiCam SVGA), with 5.7 µm pixel size, equipped with a Fujinon f1.4 /12 mm objective. Both laser and camera were synchronized by an ILA PIV-Synchronizer 2003 connected to a computer controlling the synchronizer and the camera via PIVTecILA software. Particles were generated with a vaporizer

(PALAS AGF 10.0) intermediately stored in a reservoir before entering the convection cell. Image processing was performed with commercial software (DaVis, LaVision). Therefore the raw images were background corrected by averaging the recorded 1200 double frames and subtracting the average image from each raw image to increase contrast and reduce noise. Hence the images were evaluated for an interrogation window size of 48 × 48 pixels (first two passes) and 24 × 24 pixels (three further passes) without any pre-processing. Finally, vector field averaging was used to extract flow information in order to identify dominant structures and events in the velocity field. The experimental setup is depicted in Figure 2.

To measure the thermal homogeneity of the surface of the transparent heating plate, we painted the surface of the heating plate black to ideally serve as black body thermal radiation emitter and recorded the thermal emission with an infrared (IR) camera (InfraTec VarioCAM HR) at various heating powers. Data was evaluated with appendant software (InfraTec Irbis 3 plus). Since the heating plate consisted of a double glazing (see Figure 4 a) we did the measurement for both sides of the heating plate.

Results

Initially, the applicability of the transparent heating plate was evaluated for thermal convection experiments. The herein applied transparent heating plate contained of an electrically conductive, but transparent coating on a standard window pane plate. Detailed information like utilized TCO, sheet resistance and thickness of the coating were not available. The heating element was built of a double glazing to reduce thermal loss from the backside of the heater to the environment. The cross-section of the heater is sketched in Figure 4 a). Figure 3 depicts the transmission spectrum of the transparent heating plate provided by the supplier.

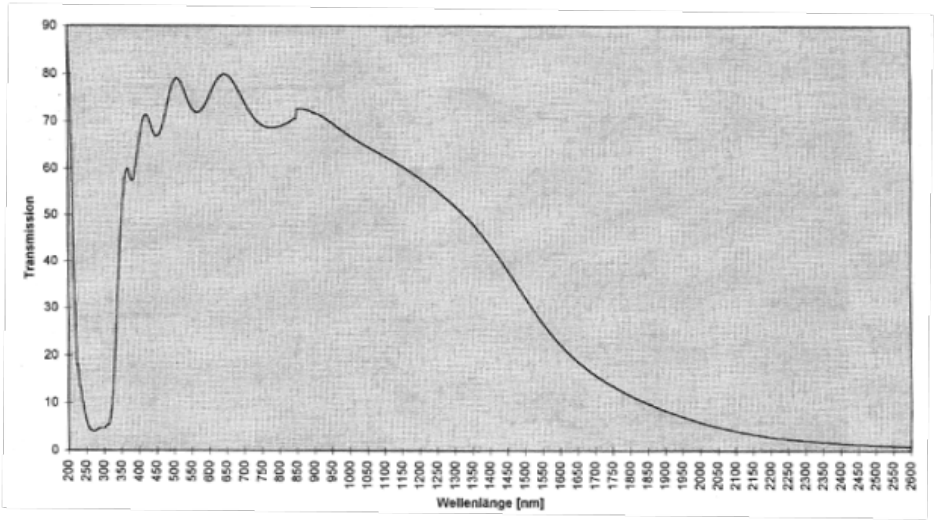

Figure 3: Transmission spectrum, T (%) vs. λ (nm), of the applied transparent heating plate HVT-2, by courtesy of Hillesheim GmbH.

Comparing the transmission spectrum to the literature it is obvious that the utilized TCO was the commonly used indium tin oxide (ITO).[14] Measuring the resistance of the ITO and connecting wires

revealed 33.6 Ω. Due to the accessible transmission range of the heater PIV application is sufficiently supported at 532 nm observation wavelength applied in the current experiment. The T_{50} transmission range of about 350 nm to 1300 nm gives further rise for future application of temperature field measurements by means of laser induced fluorescence (LIF)[15,16], thermographic phosphorescent particles (TPP)[17,18] as well as thermographic liquid crystals[19,20,21].

A further property of high importance, directing on the accuracy of thermal convection experiments, is the isothermal temperature distribution on the surface of the heating plate. Therefore we imaged the thermal radiation of the heating plate with an infrared camera and evaluated the temperature distribution on its surface. We investigated two different cases: first the heated glass plate on top (as shown in Figure 4 a) and second the heated glass plate at the bottom (upside down configuration as shown in Figure 4 a). The IR camera imaged the thermal radiation of the respective configuration always from top view to the subjacent heating plate. In both cases the side-wall frame of the convection cell was placed on top of the surface to include probable heat-sink to the frame. The IR setup is depicted in Figure 4 b).

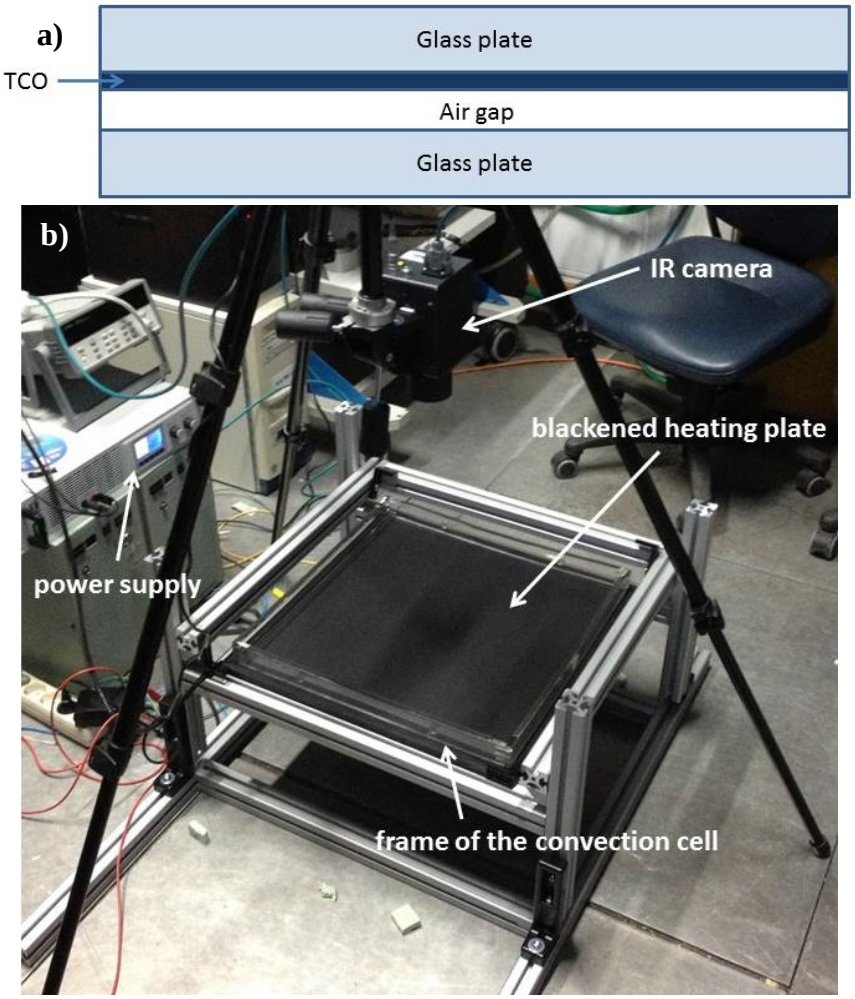

Figure 4: a) cross-section of the transparent heating plate, and b) IR setup.

The measurements were done for various heating powers: 52, 114, 200, 310, 444, 602 and 784 W (last both only for configuration with heating layer at bottom plate). Two exemplary results for front and back side of the heater at 444 W heating power are depicted in Figure 5.

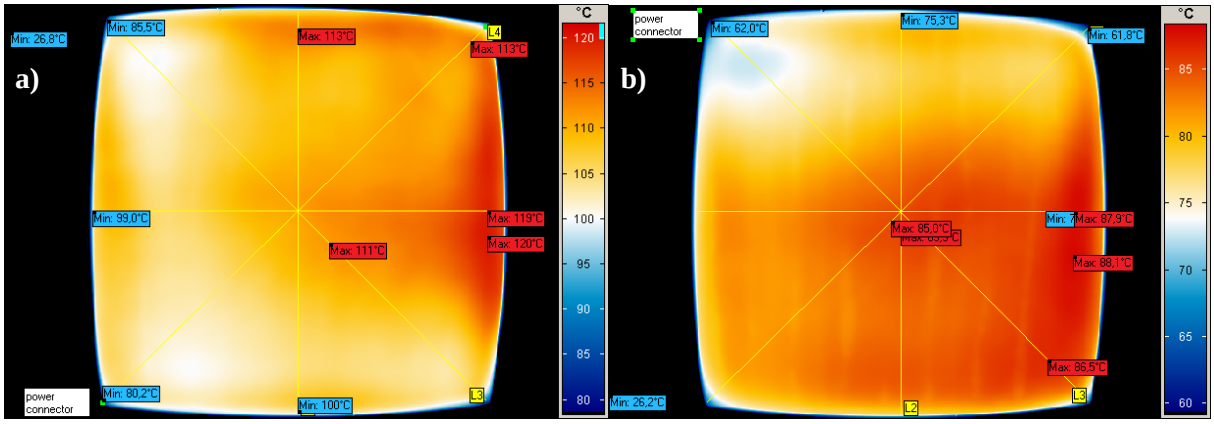

Figure 3: Infrared images of the surface of the transparent heating plate at a heating power of 444 W; a) shows the temperature distribution with heated glass plate on top, and b) shows the temperature distribution with the heated glass plate at bottom.

To evaluate the surface temperature variation the mean value T, standard deviation ΔT and maximum temperature deviation $\Delta T_{max} = T_{max} - T_{min}$ were calculated; the results are summarized in Table 1.

Table 1: Statistical evaluation of thermal distribution on the respective surface of the heating plate, temperature values are given in °C, and heating power P in W.

	heating layer at top plate					heating layer at bottom plate				
P	T	ΔT	T_{min}	T_{max}	ΔT_{max}	T	ΔT	T_{min}	T_{max}	ΔT_{max}
52	39.08	0.97	34.90	41.20	6.30	34.57	1.10	29.70	36.20	6.50
114	52.56	2.44	39.80	57.52	17.72	43.30	1.88	34.20	46.51	12.31
200	68.81	3.96	48.10	76.34	28.24	54.64	3.02	39.50	59.21	19.71
310	87.64	5.13	59.50	97.30	37.80	67.76	2.82	53.20	72.14	18.94
444	107.43	5.21	80.21	120.13	39.92	81.09	4.24	61.80	88.14	26.34
602						95.69	5.94	66.40	104.62	38.22
784						110.20	7.36	74.00	120.18	46.18

Various deviations in temperature distribution are observed. For better visualization of results, the mean temperature T was plotted as function of applied heating power and the maximum temperature deviation ΔT_{max} as function of the standard deviation ΔT, see Figure 6. Indeed the standard deviation of temperature is moderate in both configurations, but the maximum deviations are comparably large. Figure 6 b) reveals that the configuration with heating layer at the top glass plate delivers minimally better results, namely smaller standard deviation, with respect to the maximum temperature deviation and is thus the better configuration for experimental application. Conclusively the isothermal property of the heating plate is less optimal in both configurations, but will be improved in the near future.

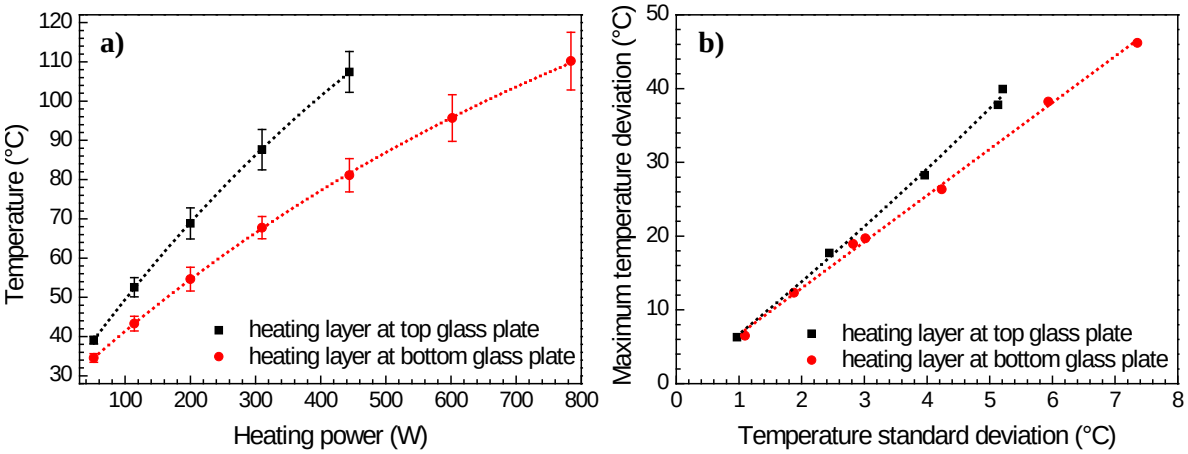

Figure 4: Statistical evaluation of data; a) shows the mean surface temperature (with error bars) as function of applied heating power, and b) shows the maximum temperature deviation as function of the standard deviation. The doted lines are exponential fits and just serve as guides to the eye.

Nevertheless, the optical transparency at PIV utilized laser wavelength of 532 nm and the more or less homogeneous surface temperature distribution gave rise to apply a first experiment in a box-shaped convection cell measuring 460 × 460 × 46 mm³. The size was chosen to be well fitting into the surface region of the heating plate with best homogeneity of temperature distribution, excluding the heat sink regions close to the edges of the heating plate. As the infrared measurements revealed better temperature distribution on the surface of the heating plate with the configuration of the heating layer at the top glass plate of the double glazing, this configuration was chosen for the initial experiment. Hence the first experiment was conducted for $Ra = 5\times10^5$ by applying 17°C at the cooling plate and 94°C at the heating plate. The experimental results of instantaneous 2d velocity fields 5 mm below the cooling plate and in mid-plane are shown on the left hand side of Figure 7. On the right hand side the corresponding DNS results are displayed. Experiment and simulation are in good agreement. Despite the less optimal isothermal condition of the transparent heating plate the experimental result is to be treated as a raving success. It seems that at larger degree of turbulence, namely large *Ra*, the instantaneous velocity fields are less affected by non-isothermal conditions of the heating plate. The flow patterns as well as the obtained velocities are very similar in both experiment and simulation. To get deeper insight into the flow dynamics, we calculated the mean velocity fields by time averaging the instantaneous velocity fields over several thousand convective time units. The result of time averaged velocity field below the cooling plate of both experimental data and DNS data for $Ra = 5\times10^5$ and $Pr = 0.71$ are depicted in Figure 8. Both results demonstrate the presence of coherent flow structures in the time averaged regime, as expected.[22,23] Since the DNS revealed highly symmetric flow pattern, the experimental data just abandoned asymmetric flow pattern. The deviation between experimental data and DNS most probably originate from the non-isothermal condition at the heating plate during the experiment, whereas the boundary conditions in DNS are ideal.

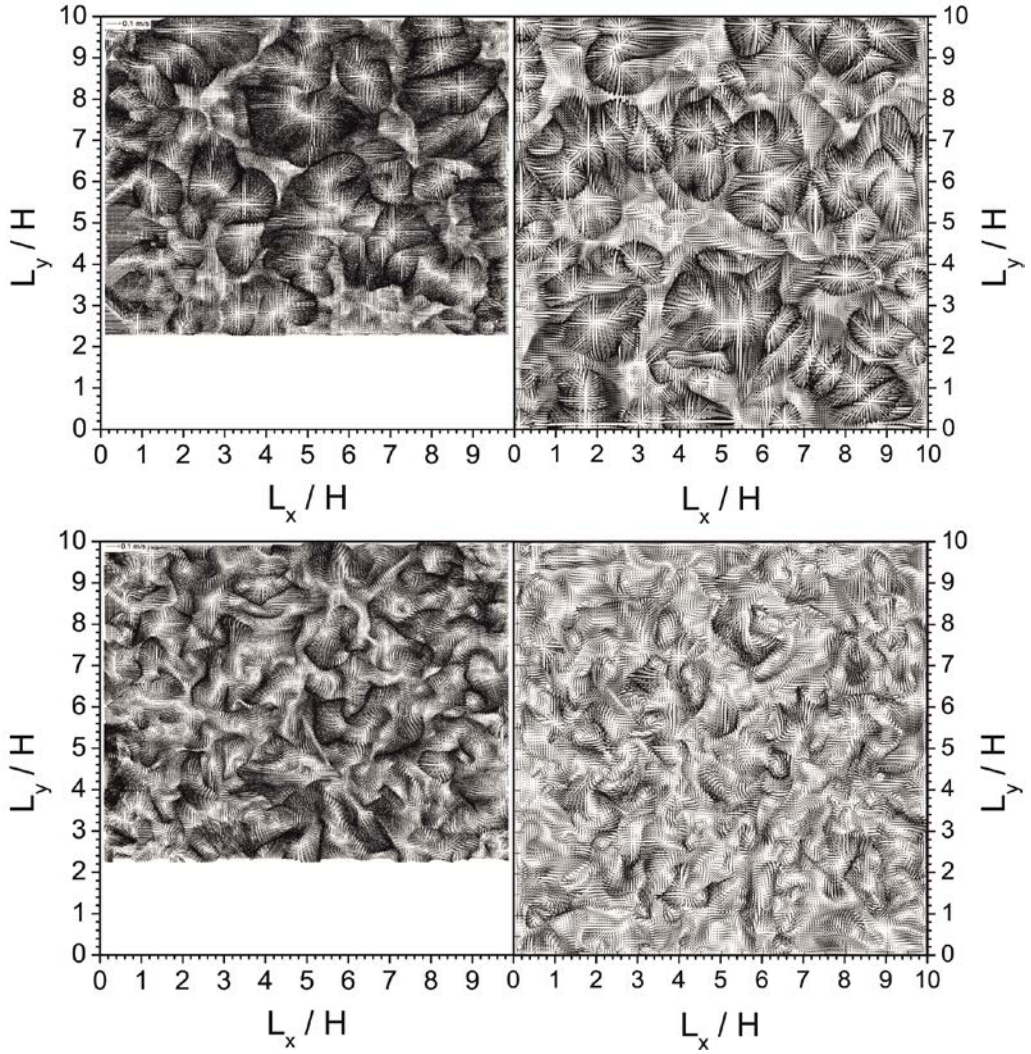

Figure 5: Visualization of instantaneous velocity fields in a horizontal plane near the top cooling plate (upper row) and in mid-plane (lower row) for $Ra = 5\times10^5$ and $Pr = 0.71$, shown are experimental 2d PIV data of 450 × 390 mm² (left) and results of DNS of 460×460 mm² (right).

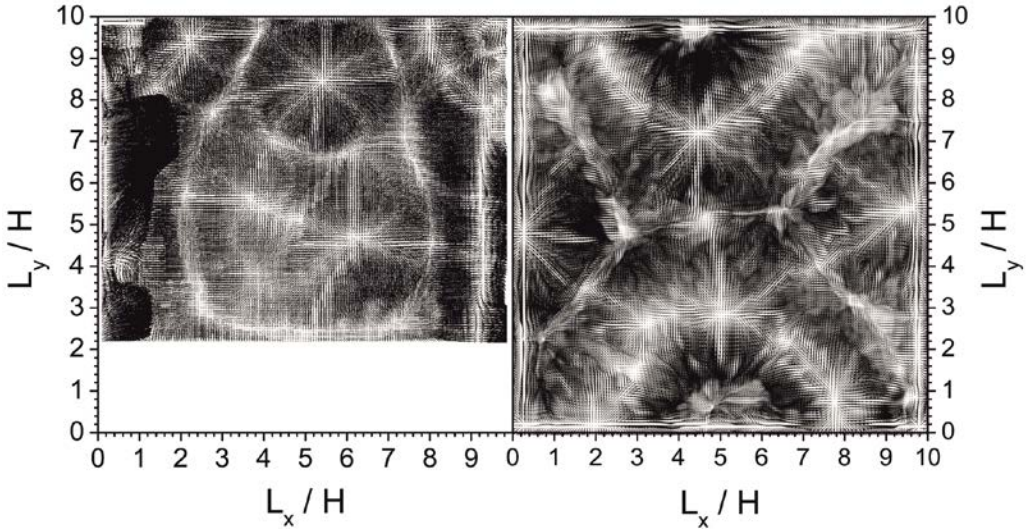

Figure 8: Time averaged velocity fields for $Ra = 5\times10^5$ and $Pr = 0.71$, below the cooling plate; left: experimental data, and right: DNS result.

Summary

We demonstrated first time application of a transparent heating plate in a Rayleigh-Bénard convection cell at large aspect ratio. The transparent heating plate revealed new insights into thermal convection by enabling the measurement of horizontal velocity fields in planes which were not accessible so far. Even though the transparent heating plate could not fully satisfy isothermal requirements, the experimental results successfully fitted the DNS results for the instantaneous velocity fields. The time averaged velocity fields unearthed coherent flow structures for both experiment and DNS, whereas only DNS yielded fully symmetric mean flow structures compared to the experiment. This result is addressed to the non-isothermal property of the transparent heating plate, which will be improved in the near future.

Acknowledgements

CK, AK and MK acknowledge financial support by the *Deutsche Forschungsgemeinschaft* DFG. The work of DK is supported by the LIMTECH Research Alliance which is funded by the Helmholtz Association. Computing resources have been provided in parts by the Scientific Big Data Analytics project SBDA003 of the John von Neumann Institute for Computing.

References

[1] **H. Bénard, J. Phys. Theor. Appl. 10 (1), 254 (1901).**

[2] **L. Rayleigh, Philosophical Magazine Series 6 32 (192), 529 (1916).**

[3] **S. Ostrach, Journal of Heat Transfer-Transactions of the Asme 110 (4B), 1175 (1988).**

[4] **L. N. Howard, Journal of Fluid Mechanics 13 (01), 158 (1962).**

[5] **R. J. Adrian, Experiments in Fluids 39 (2), 159 (2005).**

[6] **J. C. Kähler and J. Kompenhans, Experiments in Fluids 29 (1), S070 (2000).**

[7] **H. Maas, T. Putze, and P. Westfeld, in *Imaging Measurement Methods for Flow Analysis: Results of the DFG Priority Programme 1147 "Imaging Measurement Methods for Flow Analysis" 2003-2009*, edited by Wolfgang Nitsche and Christoph Dobriloff (Springer Berlin Heidelberg, Berlin, Heidelberg, 2009), pp. 53.**

[8] **G. E. Elsinga, B. Wieneke, F. Scarano, and A. Schröder, in *Particle Image Velocimetry: New Developments and Recent Applications* (Springer Berlin Heidelberg, Berlin, Heidelberg, 2008), pp. 103.**

[9] **F. Scarano, Measurement Science and Technology 24 (1), 012001 (2013).**

[10] **D. S. Ginley and C. Bright, MRS Bulletin 25 (08), 15 (2000).**

[11] **M. Tadatsugu, Semiconductor Science and Technology 20 (4), S35 (2005).**

[12] **R. Verzicco and P. Orlandi, Journal of Computational Physics 123 (2), 402 (1996).**

[13] **R. Verzicco and R. Camussi, Journal of Fluid Mechanics 477, 19 (2003).**

[14] **H. Kim, J. S. Horwitz, G. Kushto, A. Piqué, Z. H. Kafafi, C. M. Gilmore, and D. B. Chrisey, Journal of Applied Physics 88 (10), 6021 (2000).**

[15] **J. Sakakibara and R. J. Adrian, Experiments in Fluids 37 (3), 331 (2004).**

[16] **J. P. Crimaldi, Experiments in Fluids 44 (6), 851 (2008).**

[17] B. Fond, C. Abram, A. L. Heyes, A. M. Kempf, and F. Beyrau, Optics Express 20 (20), 22118 (2012).
[18] C. Abram, B. Fond, A. L. Heyes, and F. Beyrau, Applied Physics B-Lasers and Optics 111 (2), 155 (2013).
[19] D. Dabiri, Experiments in Fluids 46 (2), 191 (2009).
[20] N. Fujisawa and S. Funatani, Experiments in Fluids 29, S158 (2000).
[21] M. Ciofalo, M. Signorino, and M. Simiano, Experiments in Fluids 34 (2), 156 (2003).
[22] J. Bailon-Cuba, M. S. Emran, and J. Schumacher, Journal of Fluid Mechanics 655, 152 (2010).
[23] M. S. Emran and J. Schumacher, Journal of Fluid Mechanics 776, 96 (2015).

Karlsruhe, Germany, ISBN 978-3-9816764-2-6